Pol J Med Phys Eng. 2008;14(1):47-61.
PL ISSN 1425-4689
doi: 10.2478/v10013-008-0005-1
website: http://www.pjmpe.waw.pl

Grzegorz Taton[1], Tomasz Rok[1, 2],
Eugeniusz Rokita[1, 2]

Estimation of temperature distribution with the use of a thermo-camera

[1]Jagiellonian University Medical College, Department of Biophysics,
Sw. Lazarza 16, 31-530 Krakow, Poland
[2]Jagiellonian University, Institute of Physics,
Reymonta 4, 30-059 Krakow, Poland
e-mail: mmtaton@cyf-kr.edu.pl

The determination of three-dimensional (3D) temperature distribution within tissue during thermoablation is necessary to estimate procedure efficiency. The use of a thermo-camera combined with finite element modelling is discussed.

The temperature distributions in a metal phantom and an animal tissue sample were simulated. In the real experiment, temperatures were measured around the heating probe by a thermo-resistor set and the temperature distributions on samples' surface were acquired by a thermo-camera. The temperatures measured in the experiment were compared with the simulated ones. The differences between the measured and simulated temperatures were lower than 1.3°C and 3.0°C for a metal phantom and tissue sample, respectively.

Good agreement was achieved for homogenous material of well-defined parameters. Higher discrepancies for the tissue sample are due to in-homogeneity and to difficulties with describing tissue thermal properties.

The proposed method permits the precise prediction of a 3D temperature distribution in *in-vitro* studies. Potential application for *in-vivo* procedures requires further investigations.

Key words: finite element model, non-invasive thermometry, three-dimensional temperature distribution, thermo-camera, tissue temperature measurements.

Introduction

Thermoablation is a promising, minimally invasive method for the treatment of nonresectable tumours [4-6, 12, 13]. An adequately high temperature must be achieved in the diseased tissue to make the procedure effective. The local temperature is measured when the ablation is performed, but the temperature distribution around the probe is unknown since there are no reliable methods available for temperature three-dimensional (3D) distribution determination. Ultrasonography could be used off-line to visualize the coagulated area but the usefulness of this method is limited because of poor correlation between the real lesion size and the size seen in the image [3]. Only magnetic resonance imaging (MRI) applied during the procedure could deliver adequate image quality, but its usefulness is limited in practical applications.

A mathematical model used for calculating the tissue temperature distribution during the treatment could be a solution. Various approaches to apply Finite Elements Modelling (FEM) for ablation simulation have been made and have produced promising results [1, 7].

The presented study aims at testing the possibility of a 3D temperature distribution prediction by applying computer modelling and thermography. The main problem is tissue in-homogeneity which cannot be determined precisely without the use of a 3D imaging modality. The proposed technique as a low-cost solution may obviate this necessity, so the question arises if a 3D temperature distribution can be predicted from a surface distribution.

The FEM [2, 8-10] was used to simulate ablation performed under controlled conditions. Numerical results were compared with the experimental data obtained from a thermo-resistor set and from a thermo-camera. The experiment was made for uniform material (lead phantom) to check measurement methodology and then was repeated for horse liver *in-vitro*.

The present study is the first step in the investigations of 3D temperature distributions with the use of a thermo-camera and computer simulations in *in-vivo* procedures. The methodology tested can be used in different fields where thermoablation can be applied.

Materials and methods

Two materials were used: (1) lead — in order to test the methodology, and (2) horse liver — to simulate thermoablation under conditions close to the real situation.

A lead phantom was a $20\times10\times5$ cm^3 cuboid (Figure 1). Along the cuboid axis, a 13.5 cm-long hole designed for a probe was bored ($\Phi = 1.2$ cm). Eight holes of different depths ($\Phi = 4$ mm) were drilled for temperature sensors 10 mm under the surface and perpendicular to the probe. The probe was placed on the phantom axis and the probe tip centre was placed in the phantom centre. Since the temperature distribution in the phantom was symmetrical, the temperature sensors were placed on one side of the probe. A thermo-conductive paste was used to avoid heat loss between the phantom, sensors and probe.

A horse liver sample of about $18\times16\times4.5$ cm^3 in size was used as a tissue model. The sensors were placed at 10 to 20 mm distance from the probe on the plane containing

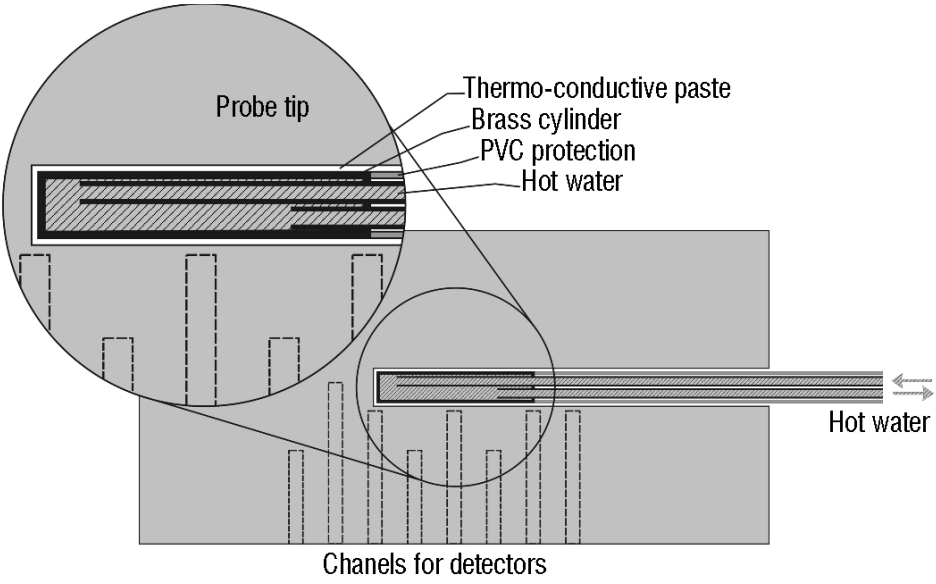

Figure 1. A schematic cross-section through the lead phantom with a heating probe. The cross-section is made along the phantom long axis, 25 mm under the surface. The positions of channels drilled 10 mm under the surface designed for thermo-resistors are also shown

the probe axis. The liver was laid flat on the table and the probe was parallel to the table (Figure 2).

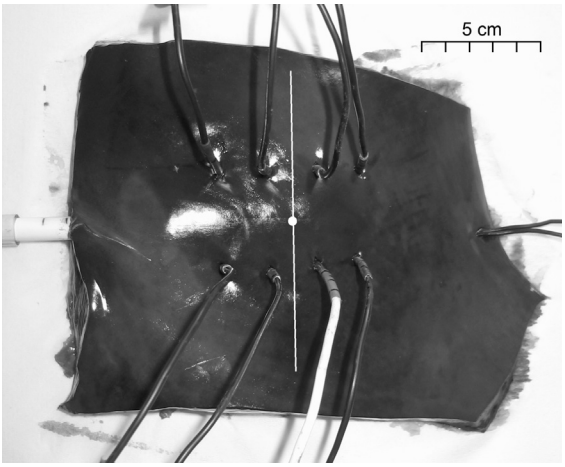

Figure 2. A horse liver phantom used in tissue investigations. Part of the heating probe is visible on the left. Eight sensors are inserted from above. The white line indicates the axis along which temperature profiles are calculated (see text). The white dot denotes axis '0'

The experimental setup

The experimental procedure adopted used a simpler system than that in clinical practice. The source of heat was a probe supplied with hot water. The probe consisted of 5 cm long brass tube ($\Phi = 10$ mm), closed on both bases (probe tip), and a PVC pipe in which two other brass pipes were used for hot water delivery and outflow (Figure 1). The water was heated in a thermostat whose temperature was 80°C.

The system applied for temperature measurements consisted of eight independent calibrated thermo-resistors (47 kΩ in 25°C), with small thermal capacity connected to a PC with a specially designed interface through a RS232C port. A 12-bit analogue-to-digital converter was used. The temperature was measured with precision of 0.1°C. The system was calibrated with a high-quality PT100 platinum thermo-resistor. The calibration procedure was performed in the temperature range between 20°C and 85°C. The same PT100 element was placed on the surfaces investigated by the thermo-camera to calibrate thermograms. The temperature time courses measured by thermo-resistors were acquired with intervals of 5 s.

The temperature distributions of the phantom surface were investigated every 2 min. The thermo-camera (V20 by VIGO, Warsaw, Poland) was placed 30 cm from the surface. The temperature of the surroundings and that of the probe tip was controlled during the whole investigation. Data were acquired over 6000 s in the case of lead phantom, and over 9000 s in the case of liver tissue. The investigations were performed until a steady-state was achieved.

Finite elements modelling

The heat transfer in the tissue is governed by a Bioheat Equation [3]:

$$\lambda \nabla^2 T = \rho c \frac{\partial T}{\partial t} - Q_s + h_{bl}\left(T - T_{bl}\right) + Q \tag{1}$$

where ρ is density [kg/m^3], c is the specific heat [J/kg/K], λ is the thermal conductivity [W/m/K], Q_s is the source of heat [W/m^3], T_{bl} is the blood temperature [K], and h_{bl} is the convective heat transfer coefficient involving blood perfusion.

The energy produced in metabolic processes (Q) is neglected as being small if compared with other terms. Since the experiment was executed *in vitro*, blood perfusion was neglected. Also tissue homogeneity was assumed. The parameters in (1) are temperature dependent. This dependence could easily be considered in numerical solutions [8, 9] but because it was secondary of importance compared with the tissue inhomogeneity assumption, ultimately constant values were adopted. The source of heat (Q_s) was defined as constantly generated heat in the whole volume of the probe tip. The assumed simplifications make the model practically useful if one considers complications involving the solution proposed and the amount of time necessary for calculations.

The probe was axially symmetrical, which would lead to an analytical solution [8] but because of the tissue sample asymmetry the FEM [10] was used to simulate the process investigated. ANSYS (ANSYS Incorp. Southpointe, USA) software was applied. The assumed boundary conditions were the consequence of experimental conditions. Heat generation was simulated by the constant temperature of the probe tip (80°C). The initial temperature of the model was equal to that of the air (24°C). The convection and radiation on the model's surface were also assumed [1, 2]. Lead and liver were

considered to be characterised by steady state thermal properties, and thus constant values of density, conductivity and heat capacity were used.

In both phantom type simulations, ten-node tetrahedral elements were used in a non-uniform mesh. The model consisted of 62300 elements in the case of the lead plate, and of 196000 elements for the final tissue simulation. The simulated time period was 6000 s for the lead and 9000 s for the liver tissue. The time step started with the value of 1 s and was automatically optimized by the software over the range between 1 and 100 s. Simulations took about 2 h for the lead plate and about 2.5 h for the liver tissue sample. A PC equipped with two Intel Xeon 2.8 GHz processors and 2 GB of RAM was used for simulations.

The agreement between the measurements and simulation results was tested with a χ^2 test. Also the correlation coefficients were calculated as a measure of agreement between temperature profiles or temperature time dependences achieved in the simulation and the experiment.

Results

The temperature time courses on each sensor were acquired in both the lead phantom and the tissue. The results were compared with the time-courses obtained in the simulations. The examples of time courses for two sensors are presented in Figure 3 for the lead phantom and in Figure 4 for the liver phantom investigations. The results are then plotted together with simulated curves. The best and the worst cases were taken for the correlation coefficients between experimental and simulated results.

The temperature distributions on the phantom surface were acquired every 120 s. The temperature distributions were simulated for the same moments. An example of a steady state temperature distribution on the liver phantom surface (after 9000 s) as a result of measurements and simulation is presented in Figure 5. In order to compare quantitatively the obtained distributions on the liver surface, temperature profiles along the horizontal phantom axis perpendicular to the probe (Figure 2) were plotted. The temperature profiles obtained in thermographic measurements were compared with the results of simulation in Figure 6.

The experiments with both phantom types were continued until a steady state was achieved on the phantom surface. In effect, the observed time courses (6000 s for the

a)

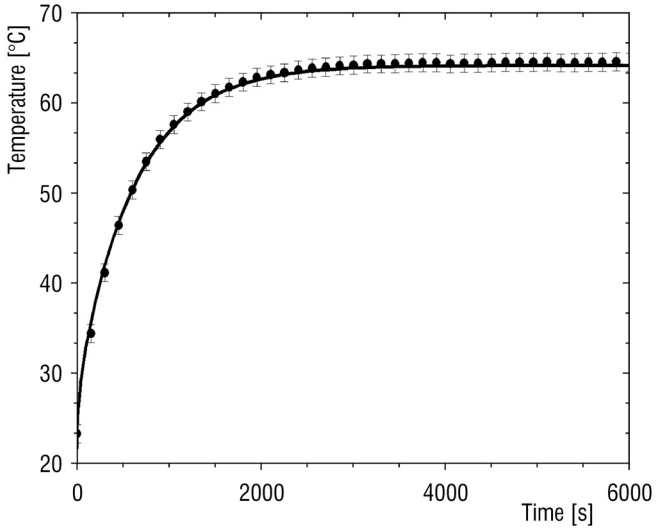

b)

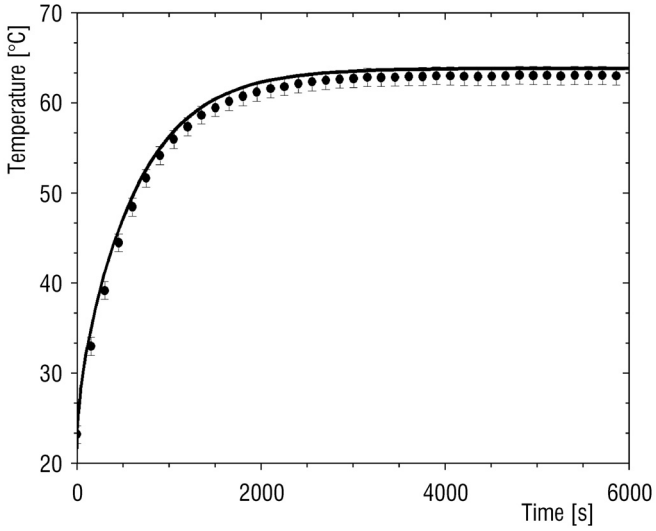

Figure 3. The measurement results obtained for two sensors in the lead phantom experiment (dots) compared with the simulated results (solid line).
The best (a) and the worst (b) cases were chosen of the correlation between the experiment and the simulation

a)

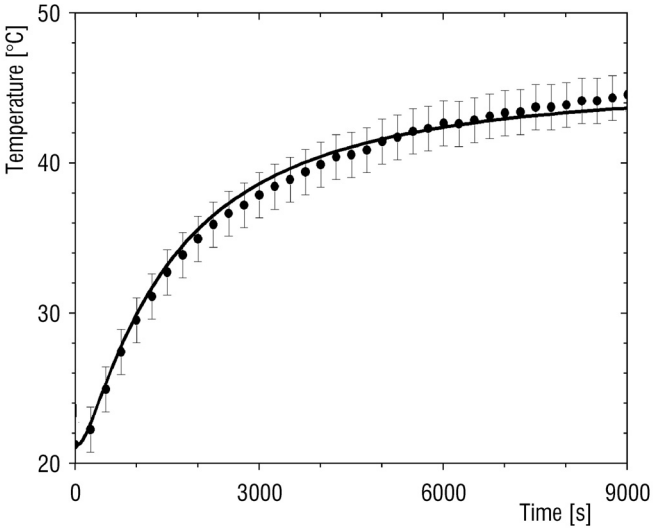

b)

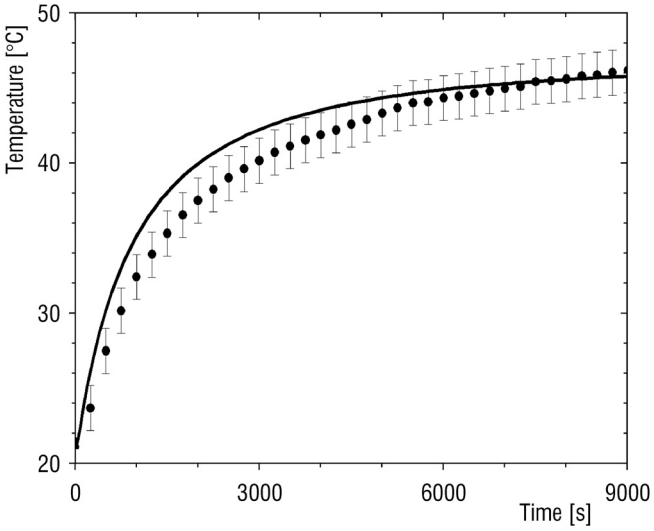

Figure 4. The measurement results obtained for two sensors in the horse liver phantom experiment (dots) compared with the simulation results (solid line). The best (a) and the worst (b) cases of the correlation between the experiment and the simulation were chosen

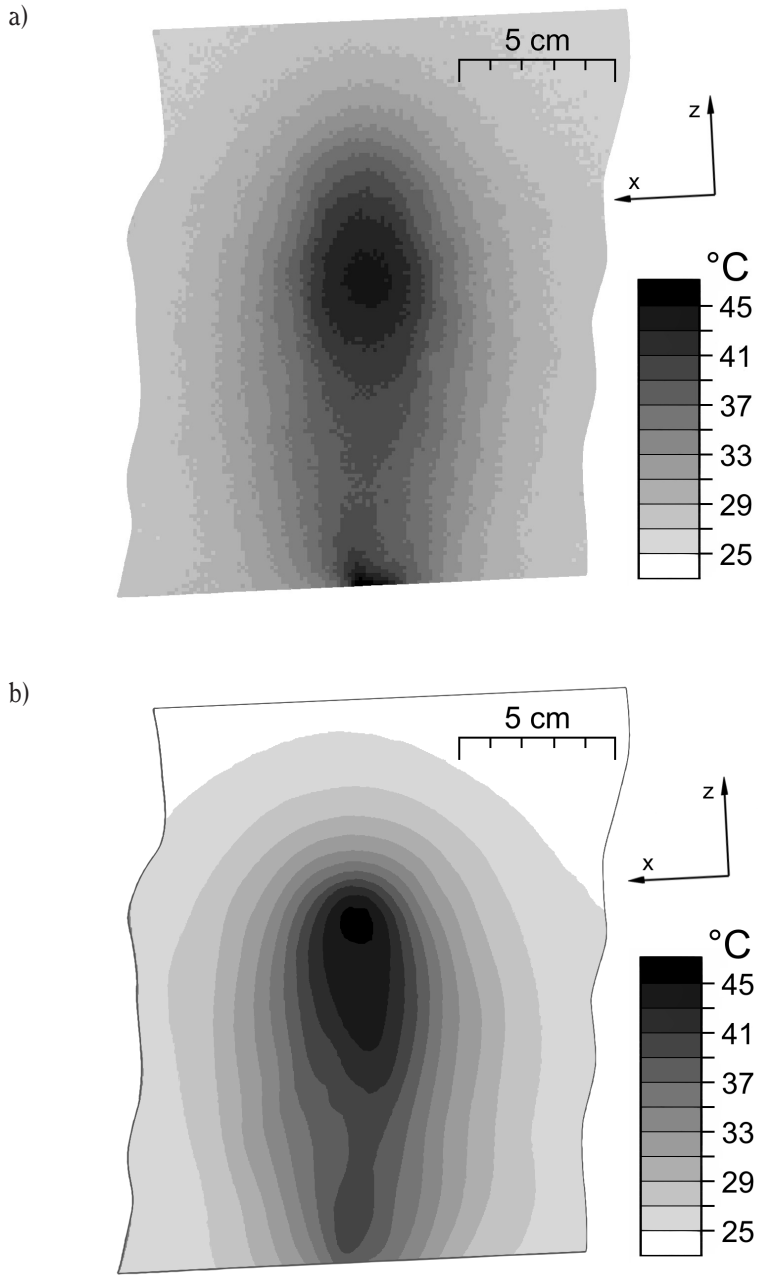

Figure 5. The temperature distributions on the horse liver surface in a steady state (after 9000 s). The thermo-camera image (a) compared with the results of simulation (b)

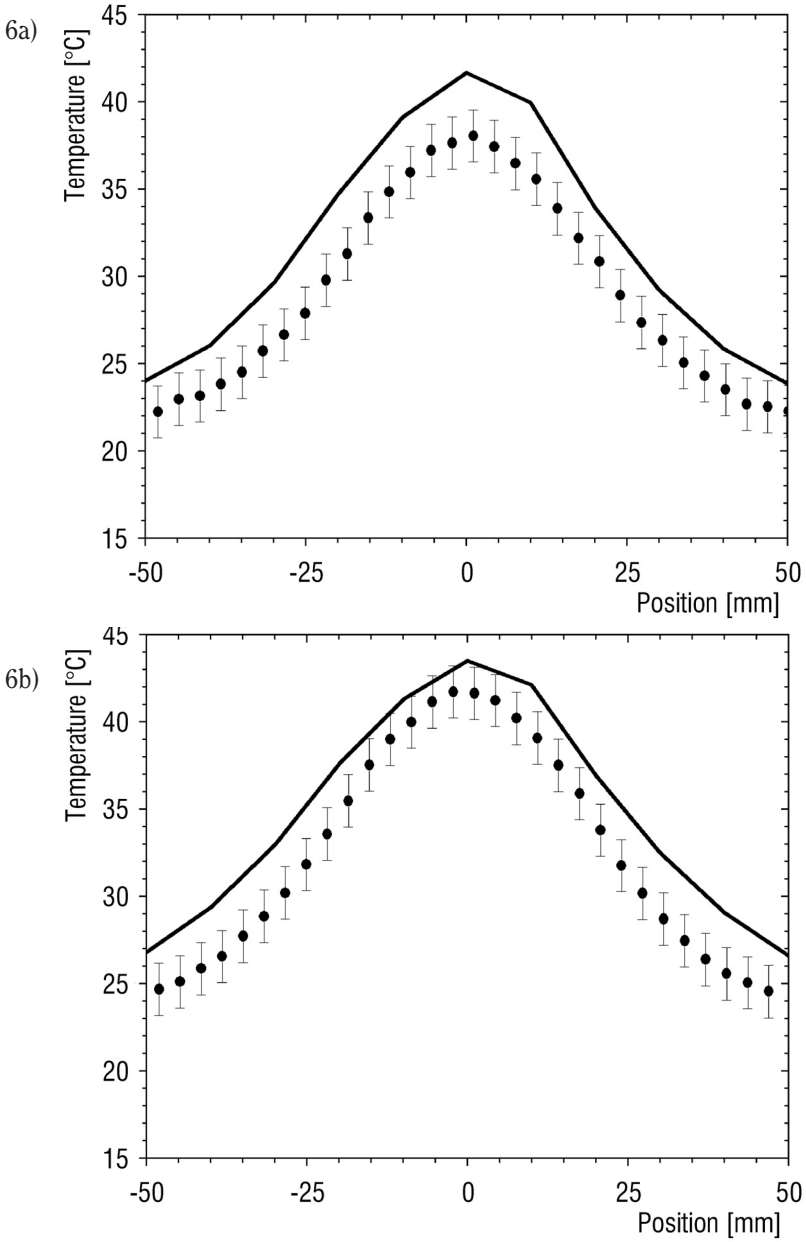

Figure 6. Temperature profiles along the horizontal axis (axis perpendicular to the probe, see Figure 2) of the liver phantom surface. After 3000 s (a), 6000 s (b) and in a steady state — after 9000 s (c). The results of thermographic measurements compared with the results of simulation. '0' is the central point of the surface

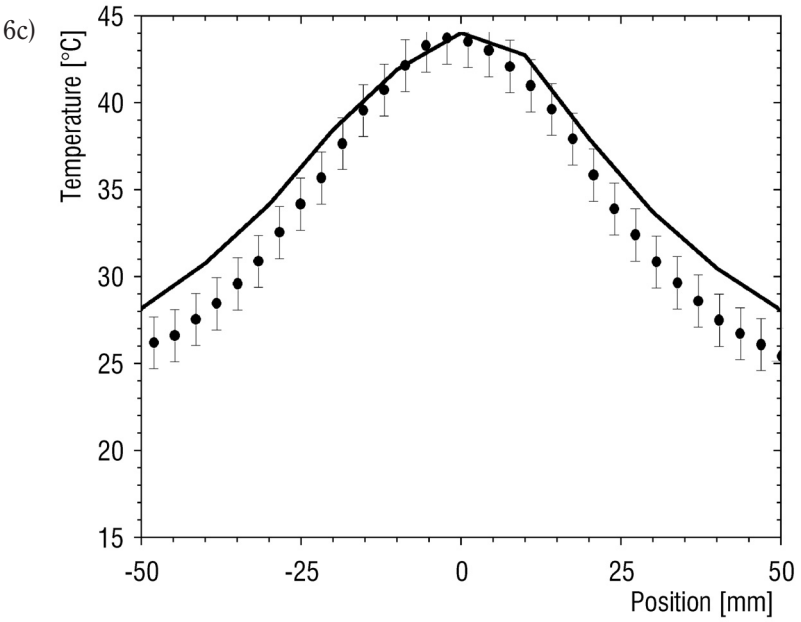

lead phantom and 9000 s for the liver tissue) are longer by a factor of 6-10 than the standard clinical procedures.

Four experiments were performed for each lead and liver phantoms. First, approaches were made to optimize the procedure. Ten to twelve simulations were made for each phantom. Most of the simulations were performed to find the best set of thermal parameters of the investigated materials. The best choice was based on the χ^2 test.

The results achieved for the lead phantom have shown that the methods used for measurements are correct. The correlation coefficient between the experimental temperature time courses measured by sensors and the curves obtained from the simulation ranged from 0.9995 to 0.9997. Also the temperature distributions acquired by the thermo-camera fitted well with simulation results. The differences between the measured and simulated temperatures on the plate surface are lower than the measurement error of about 0.9°C. The error was estimated as the deviation of the temperatures measured by the thermo-camera on the area with uniform temperature. The maximum difference of 1.3°C, higher than the measurement errors, was observed only close to the plate edges.

Higher incompatibilities were observed in the liver tissue study. The correlation coefficients between experimental and simulated time courses measured by sensors ranged from 0.990 to 0.998, and were considerably lower than those in the case of the lead phantom. This becomes clear when Figure 3 and Figure 4 are compared. For every time course acquired by particular sensors, the differences between the experiment and simulation for every time moments were calculated and subsequently the average and maximum differences were calculated for every sensor as the estimation of the discrepancy between the experiment and the simulation. The average temperature difference ranged from 0.44°C for the best case to 1.4°C for the worst one. The maximum observed range of differences was 0.9-3.0°C.

Discussion

The largest differences between the experiment and the simulation in the case of the lead plate are observed close to the plate edges. This is due to problems involving convection near the edges. Convection is still a problem which has not been solved precisely. Only simple problems such as convection of a big flat plate can be solved properly, but even in these cases phenomenological equations are applied to calculate the convection coefficients [11]. Nevertheless, by comparing the maximum observed discrepancy of 1.3°C with the temperatures range observed in thermograms (~20-65°C) a satisfactory agreement was obtained. The methodology adopted was used in the second stage of the experiment for the estimation of temperature distributions in the liver tissue.

Larger discrepancies between the measured and the simulated temperatures in the liver tissue are due to the difficulty of obtaining precise sensor positioning in the tissue in comparison with the lead phantom. The sensors were positioned without the help of any imaging method, and small errors in sensor positioning can lead to considerable temperature changes especially close to the probe. It was ascertained that the change of 2 mm in the sensor position may cause a change in the measured temperature of 1.9°C.

An analysis of surface temperature distributions for the liver tissue was performed. The measured temperature distributions are similar to those simulated ones only close to the probe. In distances farther away, the discrepancies are larger. It can easily be seen in Figure 5 and in Figure 6. The distance from the probe axis, in which the simulation and experiment agree within the experimental error, is about 15-20 mm from the axis when considering a steady state situation (Figure 6c) (15-20 mm from the axis on the

phantom surface is equivalent to about 25-30 mm from the probe axis considering the probe depth). In earlier time moments, the agreement is worse. Figures 6a and 6b clearly show temperature profiles for 3000 s and 6000 s. The temperature amplitudes are overestimated in the simulation.

Discrepancies between the experiment and the simulation in the case of tissue measurements can be explained by three factors. First and most important factor negatively affecting the results is tissue inhomogeneity. There are blood vessels present in the liver which are filled with air. This changes considerably the thermal properties of the investigated system and influences the surface temperature distribution. On the other hand, the asymmetry in the surface temperature distribution caused by large vessels has not been observed. This is probably the effect of vessels collapsing which minimizes the amount of air-filled spaces. In potential *in-vivo* studies, at least the largest blood vessels should be considered because they are filled with inflowing blood causing additional heat losses. This leads to the conclusion that imaging modality cannot be avoided for the three-dimensional tissue structure studies imaging. Another factor is the problem of convection in the lead phantom studies. The last possible source of error is the problem of definition of thermal properties of the tissue. The thermal properties of tissue change with temperature and tissue state (e.g. coagulated or not coagulated). This fact is due to the tissue structure changes and to the water loss at higher temperatures.

In accordance with the assumed simplifications, constant values for tissue thermal properties were adopted and the liver was treated as homogenous material. The best parameter values were chosen on the basis of the analysis of differences between simulations and experiments. The assumed parameter values allow good agreement for a steady state (Figure 6c). To achieve better agreement for earlier time moments (Figure 6a and Figure 6b) the parameter temperature dependences should be discovered and considered.

The simulated and investigated time durations are one order of magnitude higher than those used in practice. Such long times are unacceptable in practical solutions, but it should be emphasized that the probe used gave much lower power than clinical probes. With a more powerful probe the experiment could run shorter. This would influence also the computational time which is at present not practically acceptable.

Conclusions

The simplifications used in the computer simulations provide good agreement between the simulated and experimental data when considering homogenous material with constant values of thermal properties at variable temperatures (lead). As shown in the *in-vitro* experiment, the temperature distribution could be predicted relatively precisely in the liver tissue only close to the probe. For distances smaller than 30 mm from the probe axis, the agreement between the experiment and the simulation is good.

In order to achieve a better agreement between the measurements and the simulation, some assumed simplifications have to be avoided. The tissue inhomogeneity and tissue perfusion seem to be the most important factors. The inhomogeneity can be considered if a reliable 3D imaging modality is applied to provide information about the tissue structure. This last statement leads us to the conclusion that at the present, thermography supported by computer simulation cannot be an alternative solution as a low-cost guidance method in ablative therapy. The proposed solution works well in *in-vitro* applications.

The methodology presented was applied on the liver tissue but could easily be used with other kinds of tissue in *in-vitro* studies. *In-vivo* studies will be rather limited to applications in which the ablation is applied at relatively low depths. For example, the breast tissue would be a better location for such procedures than the liver. This conclusion, however, requires further study.

Acknowledgements

Work supported by grant 6P05C01521 from the Polish State Committee for Scientific Research

References

[1] Barauskas R, Gulbinas A, Barauskas G. Investigation of radiofrequency ablation process in liver tissue by finite element modeling and experiment. Medicina. 2007; 43: 310-325.

[2] Chang I. Finite Element Analysis of Hepatic Radiofreqiency Ablation Probes using Temperature-Dependent Electrical Conductivity. Biomed Eng OnLine. 2003; 2: 12-29.

[3] Dick E, Taylor-Robinson S, Thomas H, Gedroyc W. Ablative therapy for liver tumours. Gut. 2002; 50: 733-739.
[4] Garrean S, Hering J, Helton S, Espat J. A primer on transarterial, chemical, and thermal ablative therapies for hepatic tumors. Am J Surg. 2007; 194: 79-88.
[5] Haemmerich D, Chachati L, Wright A, Mahvi D, Lee F, Webster J. Hepatic Radiofrequency Ablation With Internally Cooled Probes: Effect of Coolant Temperature on Lesion Size. IEEE Trans Biomed Eng. 2003; 50: 493-500.
[6] Hildebrandt B, Wust P, Ahlers O, Dieing A, Sreenivasa G, Kerner T, Felix R, Riess H. The cellular and molecular basis of hyperthermia. Critical Rev Oncol Hemat. 2002; 43: 33-56.
[7] Jain M, Wolf P. A Three-Dimensional Finite Element Model of Radiofrequency Ablation with Blood Flow and its Experimental Validation. Ann Biomed Eng. 2000; 28: 1075-1084.
[8] Johnson P, Saidel G. Thermal Model for Fast Simulation During Magnetic Resonance Imaging Guidance of Radio Frequency Ablation. Ann Biomed Eng. 2002; 30: 1152-1161.
[9] Mohammed Y, Verhey F. A finite element method model to simulate laser interstitial thermo therapy in anatomical inhomogeneous regions. Biomed Eng OnLine. 2005; 4: 2-17. doi: 10.1186/1475-925X-4-2.
[10] Reddy J, Gartling D. The Finite Element Method in Heat Transfer and Fluid Dynamics. London: CRC Press; 2003.
[11] Shang D. Free Convection Film Flows and Heat Transfer. Berlin: Springer; 2006.
[12] Stauffer P, Goldberg S. Introduction: Thermal ablation therapy. Int J Hyperthermia. 2004; 20: 671-677.
[13] Strasberg S, Linehan D. Radiofrequency Ablation of Liver Tumors. Curr Probl Surg. 2003; 40: 459-498.